Supplemental Figures

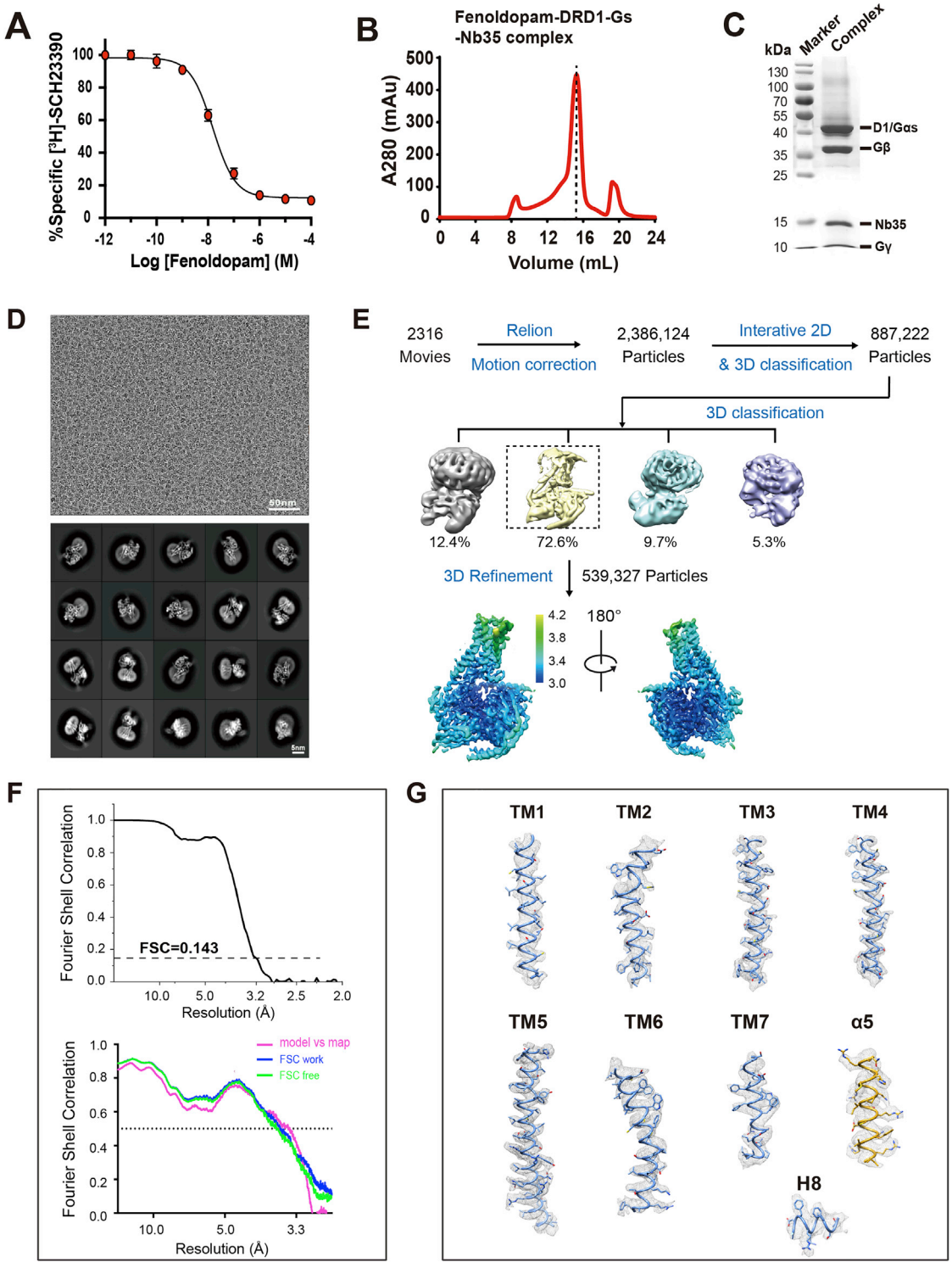

(legend on next page)

Figure S1. The fenoldopam-bound DRD1-Gs-Nb35 complex purification, cryo-EM data collection, structure determination, and cryo-EM map quality

The figures of other four DRD1-Gs with different ligands are presented in supplemental information Data S1. Related to Figure 1.

(A) Representative competitive binding curve of fenoldopam to wild-type DRD1.

(B) Representative size-exclusion chromatography elution profile of the purified Fenoldopam-DRD1-Gs-Nb35 complex using Superose 6 Increase 10/300 GL.

(C) SDS-PAGE and Coomassie blue staining analysis of the size-exclusion chromatography peak. All components of the complex could be detected by SDS-PAGE analysis.

(D) Representative micrograph (upper panel, magnification 22,500 x, defocus −1.6 μm) of fenoldopam bound DRD1-Gs-Nb35 complex, and representative 2D class average (lower panel) of the complex.

(E) Flow chart of cryo-EM data processing of fenoldopam bound DRD1-Gs-Nb35 complex including particle selection, classifications and density map reconstruction. Boxed 3D classes were selected for further processing. Cryo-EM map colored according to local resolution, which were calculated from half-maps by Relion3.0 software and generated in Chimera. Details can be found in Methods.

(F) The gold-standard Fourier shell correlation (FSC) curves for fenoldopam bound DRD1-Gs-Nb35 complex from Relion3.0 indicate overall nominal resolutions of 3.2 Å using the FSC = 0.143 criterion for the map (upper panel). Lower panel represented the cross-validation of model to cryo-EM density map. The model-versus-map FSC curves, FSC*work* and FSC*free* validation curves are shown in pink, blue, green, respectively. The marginal gap between the FSC*work* and FSC*free* curves indicates no over-fitting of the models.

(G) Representative cryo-EM density map (contoured at 0.022) and models for TM1-7, and Helix-8 of DRD1 and α5-helix of Gs_{α} in fenoldopam-DRD1-Gs-Nb35 complex.

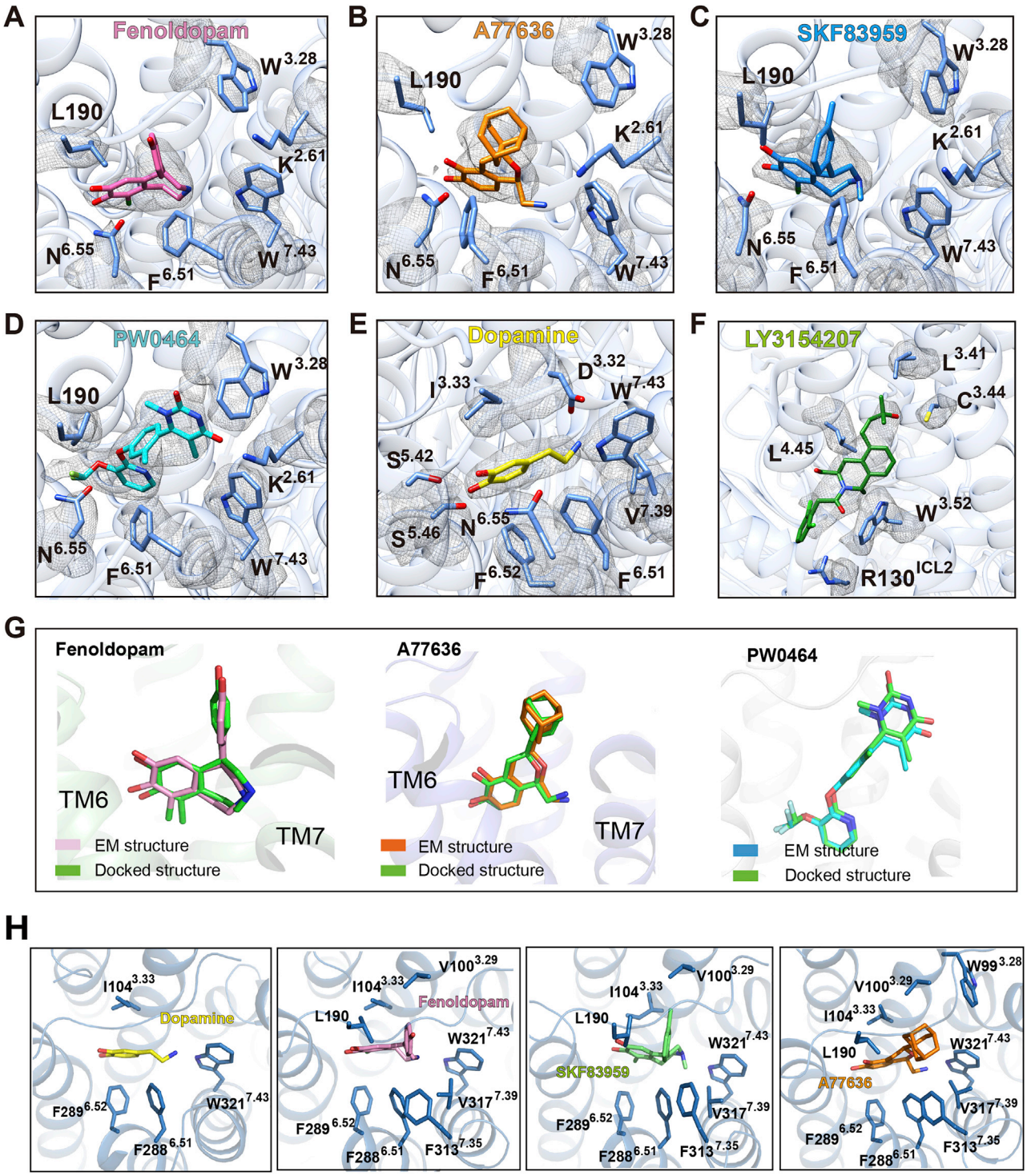

Figure S2. Detailed interaction of ligands with DRD1, related to Figure 2

(A-F) High-quality electron density facilitated unambiguous assignment of fenoldopam (A), A77636 (B), SKF83959 (C), PW0464 (D), dopamine (E) and allosteric modulator LY3154207 (F) and residues surrounding them in orthosteric binding pocket or allosteric site of DRD1. Density of the agonists are depicted as gray meshes at contour level of 0.022 except for that of SKF83959 at 0.9.

(G) To validate the binding positions of three ligands fenoldopam (left panel), A77636 (middle panel) and PW0464 (right panel), we carried out molecular docking using GLIDE. The docking results showed that the top-ranking positions of the three ligands are nearly identical to that of positioned ligands in our structures, respectively.

(H) Detailed hydrophobic interactions of DRD1 with catecholamine-based ligands dopamine (yellow), fenoldopam (pink), SKF83959 (green), and A77636 (orange), respectively. The key residues are shown as blue sticks.

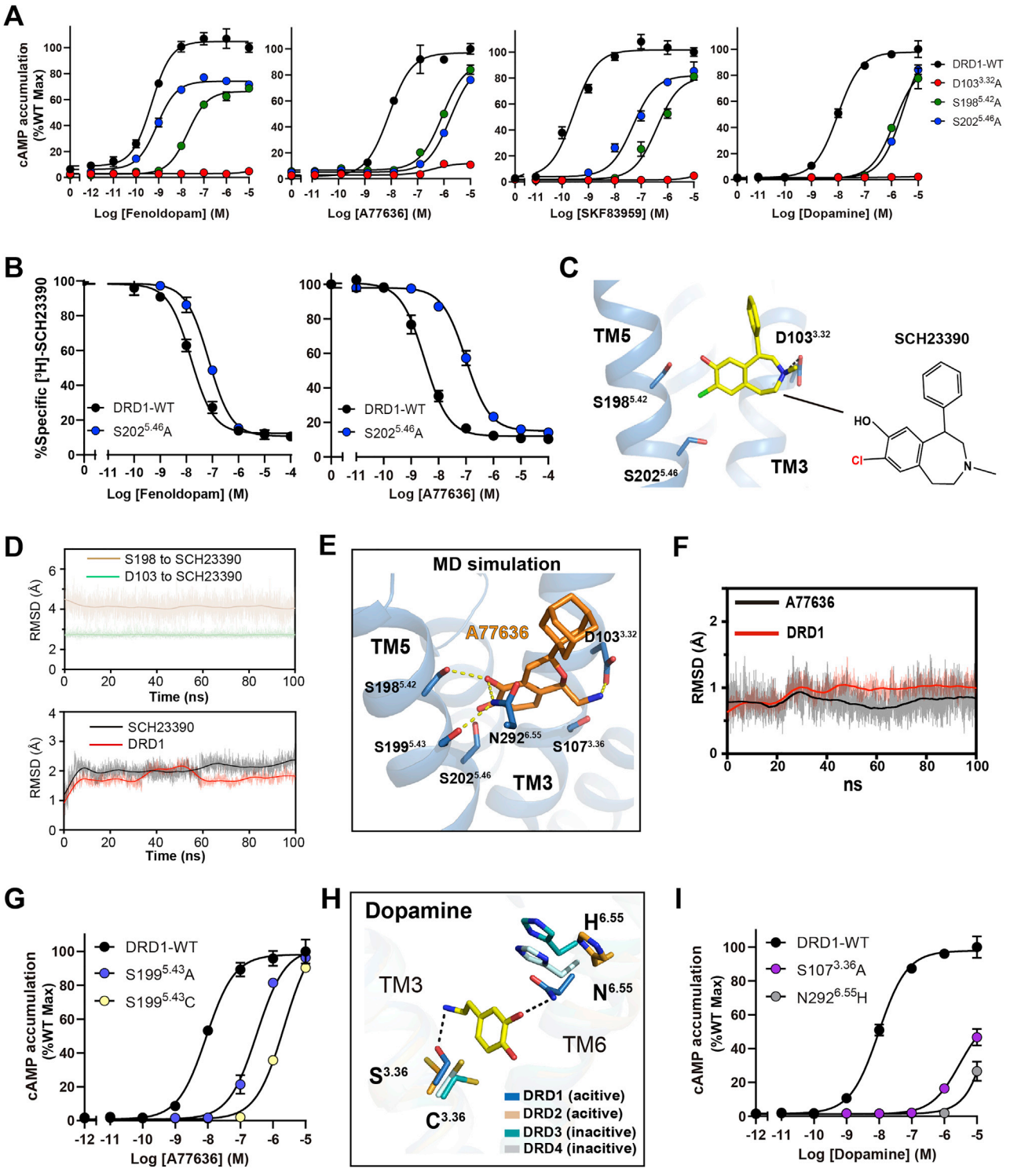

Figure S3. Function assays of OBP in DRD1, related to Figure 2

(A) Effects of the D103$^{3.32}$A, S198$^{5.42}$A and S202$^{5.46}$A mutations on agonist fenoldopam, A77636, SKF83959 or dopamine induced cAMP accumulation. Data are presented as the mean ± SEM of three independent experiments performed in triplicate.

(B) Competitive binding curves of fenoldopam (left panel) or A77636 (right panel) to wild-type DRD1 or its S202$^{5.46}$A mutant. Data are presented as the mean ± SEM of three independent experiments performed in triplicate.

(C) Chemical structure of SCH23390 and the docked model of SCH23390 bound DRD1 after 100-ns MD simulation.

(legend continued on next page)

(D) The 100-ns MD simulation course for SCH23390 bound DRD1. The upper panel shows the distance between side-chain of S198$^{5.42}$ and meta hydroxyl group of SCH23390 (light orange), and the side-chain of D103$^{3.32}$ and para hydroxyl group of SCH23390 (light green line), respectively. The lower panel displays the RMSD (root-mean-square deviation) of the ligand SCH23390 (black line) and key residues (red line) involved in SCH23390 binding in DRD1 during MD simulation.
(E) Polar interactions of DRD1 with A77636 during 100-ns MD simulation course. The residue S199$^{5.43}$ was able to form hydrogen bond with N292$^{6.55}$. The polar interactions were shown in yellow dashed lines.
(F) 100-ns MD simulation course for A77636 bound DRD1 complex. Black trace represents for the RMSD value of Cα of the DRD1 during the course, whereas red trace represents the ligand A77636.
(G) Effects of the wild-type (WT) DRD1 and its S199$^{5.43}$A and S199$^{5.43}$C mutants on A77636-induced cAMP accumulation. Data are presented as the mean ± SEM of three independent experiments performed in triplicate. See also supplemental information Data S2A for the effects of the DRD1 WT, S199$^{5.43}$A and S199$^{5.43}$C mutants on A77636, fenoldopam, SKF83959 and dopamine-induced cAMP accumulation.
(H) The S$^{3.32}$-N$^{6.55}$ pair involved in dopamine binding is shown in DRD1 structure, however, they are substituted by the C$^{3.32}$-H$^{6.55}$ pair in D2-like receptors. The polar interactions were shown in black dashed lines.
(I) Effects of the S107$^{3.36}$A and N292$^{6.55}$H mutations in DRD1 on agonist dopamine-induced cAMP accumulation. Data are presented as the mean ± SEM of three independent experiments run in triplicate.

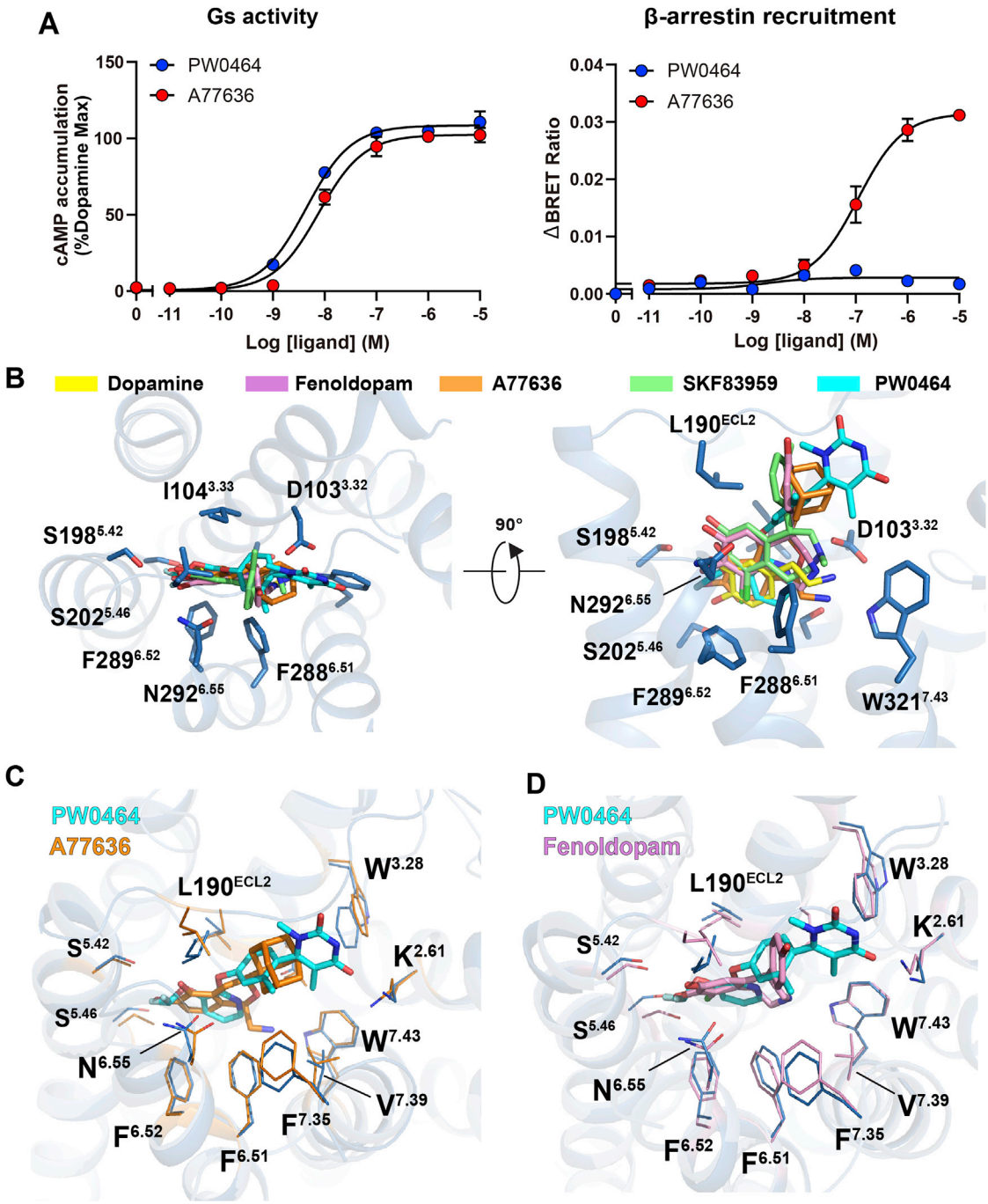

Figure S4. Comparison of PW0464 binding mode with catecholamine-based agonists in DRD1, related to Figure 3

(A) Gs-coupled cAMP accumulation assays (left panel) and β-arrestin recruitment assays (right panel) for DRD1 stimulated by PW0464 and A77636.

(B) The overlaid presentation of PW0464and four catecholamine-based agonists in OBP of DRD1 shown in extracellular view (left panel) and side view (right panel). The key residues are shown as blue sticks. Cyan, PW0464; yellow, dopamine; pink, fenoldopam; orange, A77636; green, SKF83959.

(C) Superposition of PW0464 (cyan) bound DRD1 with A77636 (orange) bound DRD1. The key residues constitute ligand binding pocket are shown as sticks with corresponding ligand color.

(D) Superposition of PW0464 (cyan) bound DRD1 with fenoldopam (pink) bound DRD1. The key residues constitute ligand binding pocket are shown as sticks with corresponding ligand color.

See also supplemental information Data S2B for the comparison of RMSD values of residues of ligand binding pocket between catechol-based agonist and non-catechol-based agonist-bound DRD1 structures. Data S2C for MD simulation course for PW0464 bound DRD1structure.

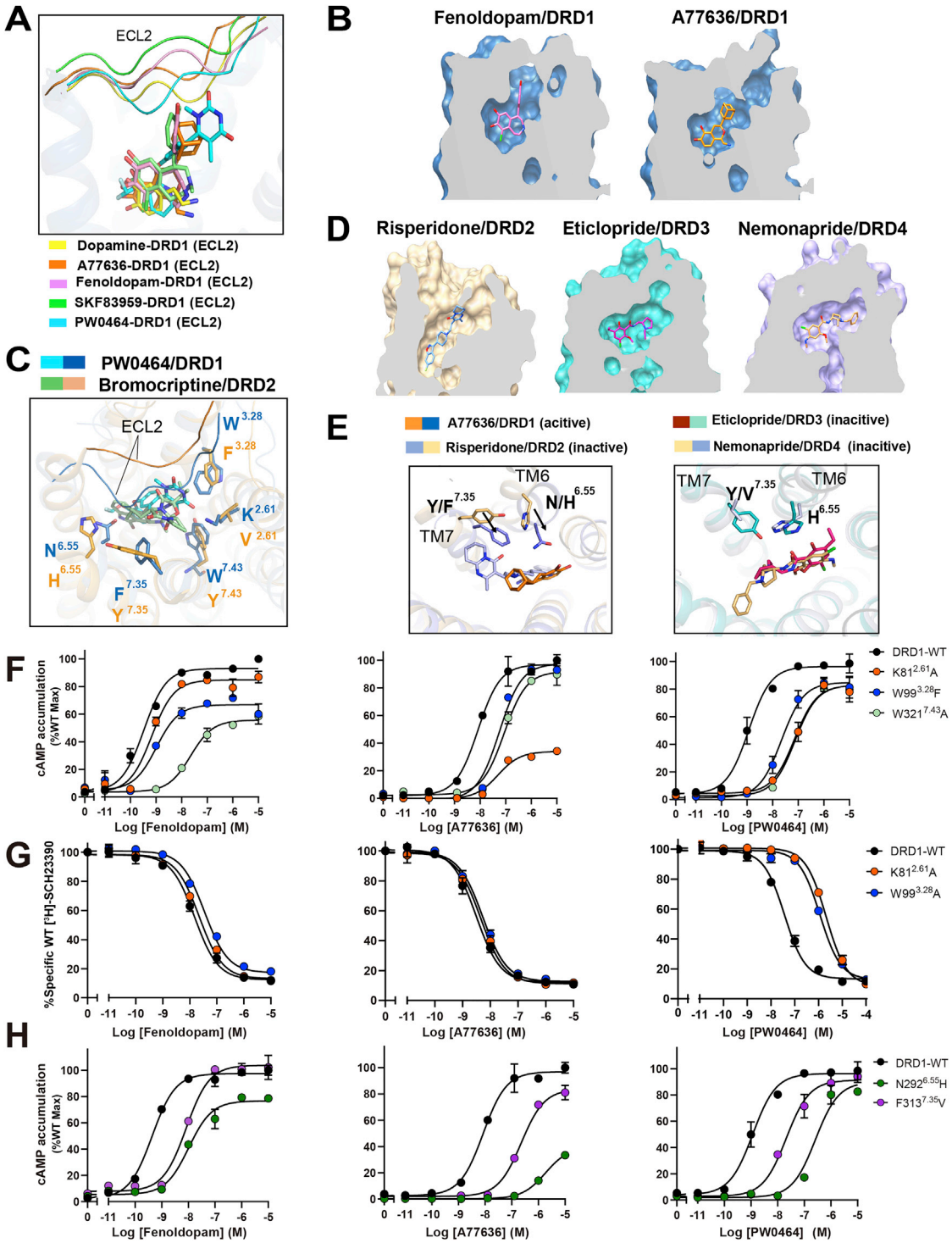

Figure S5. Structural comparison of EBP in DRD1 structures and with D2-like receptors, related to Figure 4

(A) The overlaid presentation of dopamine (yellow), A77636 (orange), fenoldopam (pink), SKF83959 (green) and PW0464 (cyan) in orthosteric binding pocket of DRD1. The difference in the ECL2 region in DRD1 complex structures was highlighted. See also supplemental information Data S2D for the comparison of RMSD values of different agonists bound DRD1 structures.

(B) Sliced surface representation of the ligand binding pocket of fenoldopam (left panel) and A77636 (right panel) bound DRD1 structures. Blue, DRD1; pink, fenoldopan; orange, A77636.

(legend continued on next page)

(C) Structural comparison of EBP in PW0464 (cyan) -DRD1(sky blue) with that in Bromocriptine (pale green) -DRD2 (orange). $K^{2.61}$-$W^{3.28}$-$W^{7.43}$ motif and $N^{6.55}$-$F^{7.35}$ motif of DRD1 are shown as sticks with corresponding color, and the equivalent motifs in DRD2 ($V^{2.61}$-$F^{3.28}$-$Y^{7.43}$ motif and $H^{6.55}$-$Y^{7.35}$ pair) are displayed as orange sticks.
(D) Sliced surface representation of the ligand binding pocket in inactive D2-like receptors. Yellow, DRD2; cyan, DRD3; slate, DRD4.
(E) $H^{6.55}$-Y/$V^{7.35}$ residues pair of D2-like receptors (right panel) involved in ligand recognition was replaced by $N^{6.55}$-$F^{7.35}$ pair in DRD1 (left panel).
(F) Effects of the K81$^{2.61}$A, W99$^{3.28}$F and W321$^{7.43}$A mutations in DRD1 on agonist fenoldopam (left panel), A77636 (middle panel) or PW0464 (right panel) induced cAMP accumulation. Data are presented as the mean ± SEM of three independent experiments performed in triplicate.
(G) Competition binding curves of fenoldopam (left panel), A77636 (middle panel) or PW0464 (right panel) to wild-type DRD1 or its K81$^{2.61}$A, W99$^{3.28}$F mutants. Data are presented as the mean ± SEM of three independent experiments performed in triplicate.
(H) Effects of the N292$^{6.55}$H and F313$^{7.35}$V mutations in DRD1 on agonist fenoldopam (left panel), A77636 (middle panel) or PW0464 (right panel) induced cAMP accumulation. Data are presented as the mean ± SEM of three independent experiments performed in triplicate.

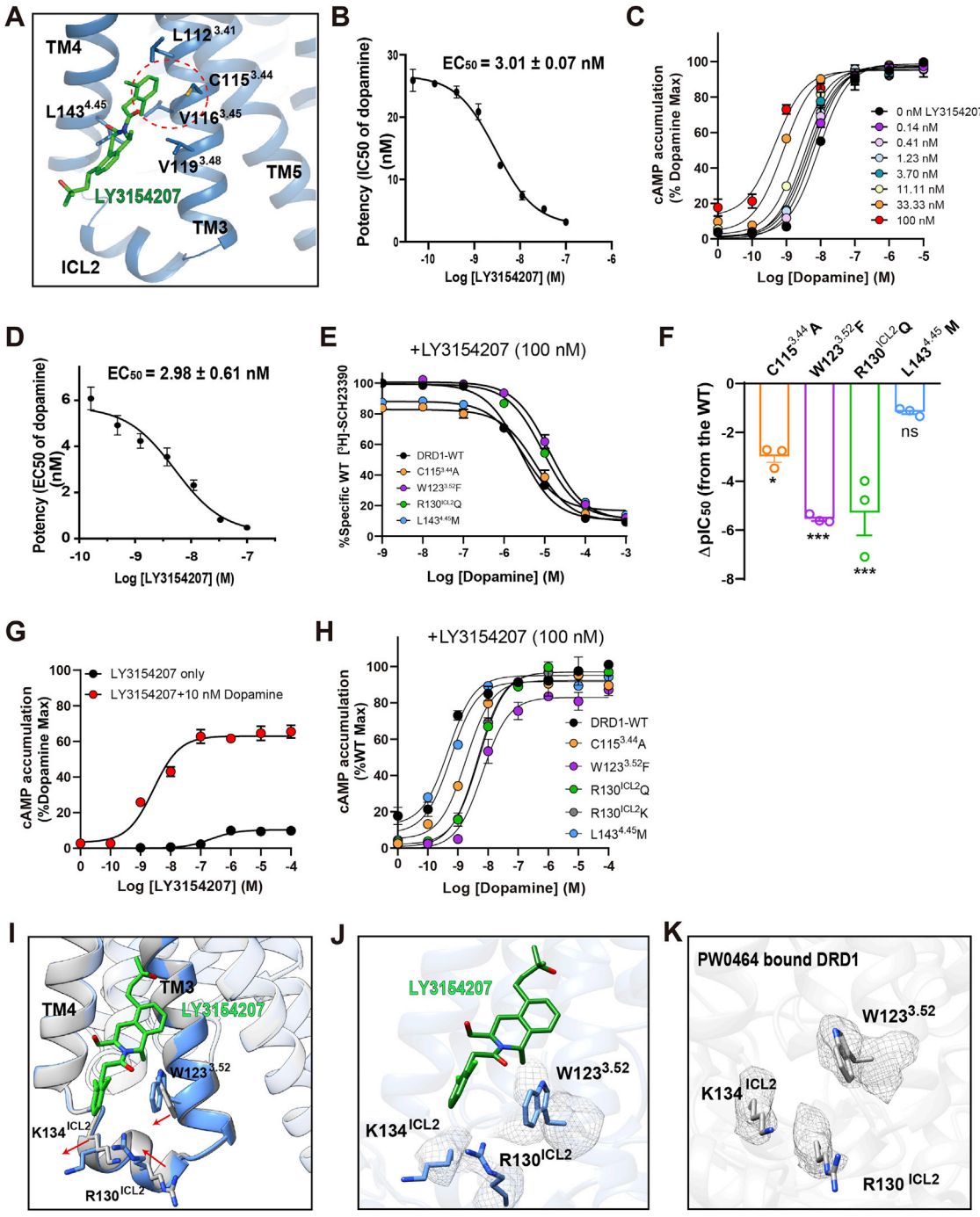

Figure S6. Allosteric modulation of LY3154207, related to Figure 5

(A) Another pose (pose 2) of LY3154207 (green) in DRD1 (sky blue). Note that the aromatic group of LY3154207 is close to the transmembrane core of the receptor (indicated by red dashed circle), which formed hydrophobic contacts with V116$^{3.45}$. Contact residues in DRD1 within 4 Å of the LY3154207 are shown as blue sticks.

(B) Competition ligand binding assay. The allosteric potency of LY3154207 on dopamine binding with DRD1 was determined. The EC_{50} of LY3154207 is 3.01 ± 0.07 nM. Data are presented as the mean ± SEM of three independent experiments performed in triplicate. This figure is related to Figure 5C.

(C) The allosteric effect of LY3154207 on DRD1-WT were determined by cAMP accumulation assay induced by dopamine. Dose dependent curves were shown. Data are presented as the mean ± SEM of three independent experiments performed in triplicate.

(D) The allosteric potency of LY3154207 on dopamine-induced DRD1 activation is determined using data from Figure S6C. The EC_{50} of LY3154207 is 2.98 ± 0.61 nM. Data are presented as the mean ± SEM of three independent experiments performed in triplicate.

(legend continued on next page)

(E) Competitive binding curves of dopamine to DRD1 wild-type or corresponding mutants in the presence of 100 nM LY3154207. Data are presented as the mean ± SEM of three independent experiments performed in triplicate.
(F) Competition ligand binding assay. Bars represent differences in calculated potency of dopamine (pIC_{50}) for each mutant relative to WT of DRD1 in the presence of 100 nM LY3154207. ***$p < 0.0001$ [one-way analysis of variance (ANOVA) followed by the Dunnett's test, compared with the response of WT].
(G) cAMP accumulation assay induced by LY3154207 in the presence or absence of EC_{20} concentration of 10 nM dopamine. The EC_{50} value (2.7 ± 0.2 nM) of PAM was shifted to left in the presence of dopamine. Data are presented as the mean ± SEM of three independent experiments performed in triplicate.
(H) Dopamine-induced cAMP accumulation assay in the presence of 100 nM LY3154207. Dose-dependent curves of DRD1 WT, $C115^{3.44}A$, $W123^{3.52}F$, $R130^{ICL2}Q$ and $L143^{4.45}M$ mutants in response to dopamine stimulations were shown. Data are presented as the mean ± SEM of three independent experiments performed in triplicate.
(I) Structural comparison reveals side-chain conformation changes of $W123^{3.52}$ and $R130^{ICL2}$ upon LY3154207 binding. Side chains of $W123^{3.52}$, $R130^{ICL2}$ and $K134^{ICL2}$ are shown in blue sticks and gray sticks in LY3154207-dopamine bound DRD1 and PW0464 bound DRD1 respectively. Note that we observed the existence of an extra density surrounding the ICL2 region of DRD1 with dopamine-LY3514207-Gs complex. The allosteric modulator LY3154207 could also be placed in this density, indicate a potential binding position during the entering of the PAM into the allosteric site. Corresponding discussion was shown in Figure S6J.
(J-K) The densities (contoured at 0.022) of $W123^{3.52}$, $R130^{ECL2}$ and $K134^{ECL2}$ in LY3514207 and dopamine-bound (J) or PW0464-bound (K) DRD1 complex shown as gray meshes are overlaid with corresponding residues.

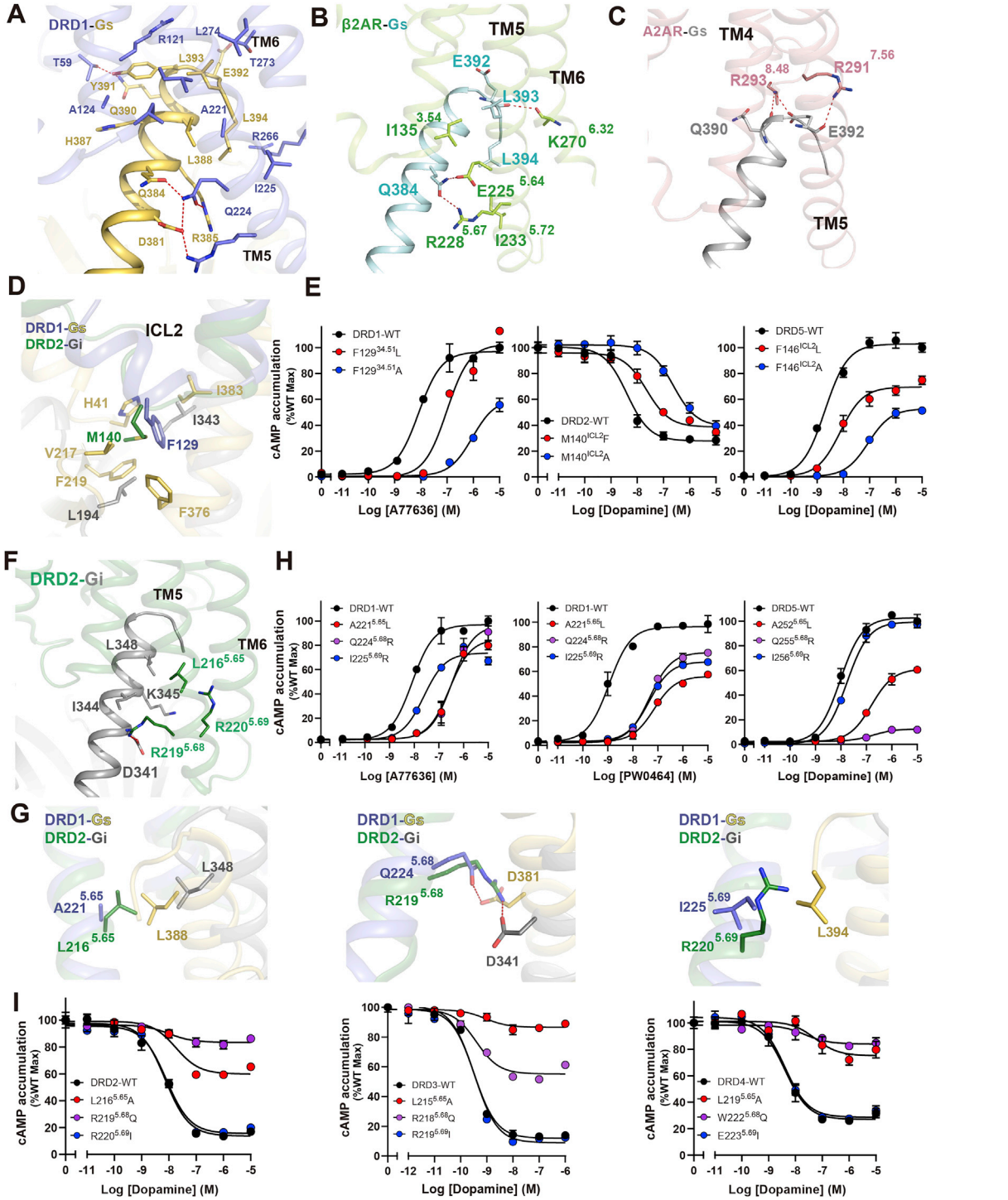

Figure S7. Comparison interface of DRD1-Gs protein with other receptors-G proteins, related to Figure 7

(A-C) Closed-up view of the interactions between the C-terminal α5-helice of $G\alpha_s$ and DRD1 (A), β2AR (B, 3S6N), and A2AR (C, 6GDG).

(D) Structural comparison of ICL2 of DRD1 (blue)-Gs (yellow) with DRD2 (green)-Gi (gray). F129 in DRD1 and equivalent residue M140 in DRD2 are shown as sticks by corresponding color, and the residues involved in F129 in DRD1 and M140 in DRD2 are shown as sticks. The structure superposition is based on alignment of TM3-helixes of DRD1 and DRD2.

(E) Effects of the F129 mutations in DRD1 and the equivalent residue M140 mutations in DRD2, as well as F146 mutations in DRD5 on agonists induced cAMP accumulation assays. Data are presented as the mean ± SEM of three independent experiments performed in triplicate. See also supplemental information Data S2F for the effects of the $V136^{ICL2}$ mutations in DRD3 and the equivalent residue $L141^{ICL2}$ mutations in DRD4 on agonists induced cAMP accumulation assays.

(legend continued on next page)

(F) Detailed interaction between α5 helix in $G\alpha_i$ (gray) and DRD2 (blue). Polar interaction is highlighted as a red dashed line. The key $L^{5.65}xxR^{5.68}$ motif of DRD2 involved in G protein coupling is presented in green stick.

(G) Comparison of the structural equivalent interactions in receptor-G protein interface in D1D1-Gs and DRD2-Gi complexes. Structural equivalent interactions between residues of $A221^{5.65}$ (DRD1) and L348 ($G\alpha_s$), $L216^{5.65}$ (DRD2) andL388 ($G\alpha_i$) (left panel); $Q224^{5.68}$ (DRD1) and D381 ($G\alpha_s$), $R219^{5.68}$ (DRD2) and D341 ($G\alpha_i$) (middle panel); $I225^{5.69}$ (DRD1) and L394 ($G\alpha_s$), R (right panel) are shown when the TM3-helixes of DRD1 and DRD2 were aligned. The polar interactions are indicated as red dashed lines.

(H) Effects of the $A^{5.65}L$, $Q^{5.68}R$, and $I^{5.69}R$ mutations in D1-like receptors (DRD1 and DRD5) on agonists induced cAMP accumulation. Data are presented as the mean ± SEM of three independent experiments performed in triplicate.

(I) Effects of the equivalent $L^{5.65}A$, $R^{5.68}Q$ and $R^{5.69}L$ mutations in D2-like receptors (DRD2, DRD3 and DRD4) on dopamine induced activation respectively. Data are presented as the mean ± SEM of three independent experiments performed in triplicate.